



# Direct visualization of translational GTPase factor pool formed around the archaeal ribosomal P-stalk by high-speed AFM

Hirotsu Imai<sup>a,1</sup> , Toshio Uchiumi<sup>b,1</sup> , and Noriyuki Kodera<sup>a,1</sup> 

<sup>a</sup>Nano Life Science Institute (WPI-NanoLSI), Kanazawa University, Kakuma-machi, 920-1192 Kanazawa, Japan; and <sup>b</sup>The Institute of Science and Technology, Niigata University, Ikarashi 2-8050, Nishi-ku, Niigata 950-2181, Japan

Edited by Peter B. Moore, Yale University, New Haven, CT, and approved November 9, 2020 (received for review September 14, 2020)

**In translation elongation, two translational guanosine triphosphatase (trGTPase) factors EF1A and EF2 alternately bind to the ribosome and promote polypeptide elongation. The ribosomal stalk is a multimeric ribosomal protein complex which plays an essential role in the recruitment of EF1A and EF2 to the ribosome and their GTP hydrolysis for efficient and accurate translation elongation. However, due to the flexible nature of the ribosomal stalk, its structural dynamics and mechanism of action remain unclear. Here, we applied high-speed atomic force microscopy (HS-AFM) to directly visualize the action of the archaeal ribosomal heptameric stalk complex, aP0•(aP1•aP1)<sub>3</sub> (P-stalk). HS-AFM movies clearly demonstrated the wobbling motion of the P-stalk on the large ribosomal subunit where the stalk base adopted two conformational states, a predicted canonical state, and a newly identified flipped state. Moreover, we showed that up to seven molecules of archaeal EF1A (aEF1A) and archaeal EF2 (aEF2) assembled around the ribosomal P-stalk, corresponding to the copy number of the common C-terminal factor-binding site of the P-stalk. These results provide visual evidence for the factor-pooling mechanism by the P-stalk within the ribosome and reveal that the ribosomal P-stalk promotes translation elongation by increasing the local concentration of translational GTPase factors.**

ribosome | ribosomal P-stalk | translation elongation | trGTPase | HS-AFM

The ribosome translates genetic information by interacting with various translational guanosine triphosphatase (trGTPase) factors in each step of translation (initiation, elongation, termination, and recycling). Translation elongation is mediated by two trGTPases: EF1A (EF-Tu in bacteria), which delivers aminoacyl-transfer RNA (aa-tRNA) to the ribosomal A site; and EF2 (EF-G in bacteria), which catalyzes translocation (1, 2). EF1A and EF2 alternately bind to a common binding site, the factor-binding center of the ribosome, and dissociate upon GTP hydrolysis. In this process, EF1A has to continuously deliver aa-tRNA to the A-site until the ribosome accepts the cognate aa-tRNA. In order to efficiently repeat these EF1A- and EF2-dependent steps in accurate translation elongation, ribosomes possess a delicate molecular equipment for binding and dissociation of EF1A and EF2.

A set of ribosomal proteins, which is called the “stalk,” plays a crucial role in the recruitment of trGTPases to the factor-binding center and the activation of subsequent GTP hydrolysis (3–5). Previous biochemical studies revealed that the *Escherichia coli* (*E. coli*) ribosomal L12 stalk allows the association of the EF-Tu•GTP•aa-tRNA ternary complex and EF-G•GTP with the ribosome to take place more rapidly than would be expected by free diffusion (6, 7). The ribosomal stalk is conserved in all domains of life and present in the large subunit of the ribosomes (*SI Appendix, Fig. S1*). In archaea, one copy of the ribosomal protein aP0 binds directly to the 23S ribosomal RNA, and three homodimers of the stalk protein aP1 form the heptameric aP0•(aP1•aP1)<sub>3</sub> P-stalk complex (8, 9). In eukaryotes, the ribosomal protein P0 associates with two P1•P2 heterodimers to form the P0•(P1•P2)<sub>2</sub> P-stalk complex, while the bacterial ribosomal L12

stalk are formed by the association of bL10 and two or three bL12 homodimers (4, 10). aP1 consists of three domains: the N-terminal dimerization domain which is also required for binding to aP0, the flexible hinge, and the C-terminal region which directly binds to each trGTPase (11–14). A C-terminal region homologous to aP1 is also present in aP0, and, thus, the archaeal aP0•(aP1•aP1)<sub>3</sub> P-stalk has seven binding sites for the trGTPases. Sequence comparison shows that the archaeal aP1 and eukaryotic P1/P2 stalk proteins are homologous to each other. However, aP1 and P1/P2 show little similarity to the bacterial stalk protein bL12 (15), although they play a common role in mediating the efficient turnover of trGTPases.

Isolated ribosomal stalks have been well characterized by biochemical and structural analyses, whereas their mechanism of action and structure-function relationship in the ribosome-bound states are poorly understood. Although early electron micrographs (EMs) identified a stalklike protrusion composed of bL12 on the *E. coli* 50S subunit (16–18), in recent structural studies, such as X-ray crystallography and cryo-EM, the overall structure of the ribosomal stalk has not been detected due to its flexible nature (19–23). To date, only part of the C-terminal domain of bL12, which bound to EF-Tu or EF-G on the factor-binding center, has been visualized in several structural studies (24–29). Therefore, our knowledge about the binding dynamics between

## Significance

Translation of genetic information by the ribosome is a core biological process in all organisms. The ribosomal stalk is a multimeric ribosomal protein complex which plays an essential role in translation elongation. However, the working mechanism of the ribosomal stalk still remains unclear. In this study, we applied HS-AFM to investigate the working mechanism of the archaeal ribosomal P-stalk. HS-AFM movies demonstrate that the P-stalk collects two translational GTPase factors (trGTPases), aEF1A and aEF2, and increases their local concentration near the ribosome. These direct visual evidences show that the multiple arms of the ribosomal P-stalk catch the trGTPases for efficient protein synthesis in the crowded intracellular environment.

Author contributions: H.I., T.U., and N.K. designed research; H.I. and N.K. performed research; H.I. and N.K. contributed new reagents/analytic tools; H.I. and N.K. analyzed data; and H.I., T.U., and N.K. wrote the paper.

The authors declare no competing interest.

This article is a PNAS Direct Submission.

This open access article is distributed under [Creative Commons Attribution-NonCommercial-NoDerivatives License 4.0 \(CC BY-NC-ND\)](https://creativecommons.org/licenses/by-nc-nd/4.0/).

See [online](#) for related content such as Commentaries.

<sup>1</sup>To whom correspondence may be addressed. Email: himai@staff.kanazawa-u.ac.jp, uchiumi@bio.sc.niigata-u.ac.jp, or nkodera@staff.kanazawa-u.ac.jp.

This article contains supporting information online at <https://www.pnas.org/lookup/suppl/doi:10.1073/pnas.2018975117/-DCSupplemental>.

First published December 7, 2020.

free trGTPases and their multiple binding sites on the ribosomal stalk is extremely limited.

At least, two mechanistic functions of the ribosomal stalk have been discussed (5). One is the factor-pooling function in which the multiple arms of the ribosomal stalk recruit trGTPases to the factor-binding center by binding and thereby increasing the local concentration of trGTPases (4, 9). The other is an ability to bind and stabilize trGTPases associated with the sarcin/ricin loop of 23/28S ribosomal RNA (rRNA), which catalyzes GTP hydrolysis (30). Importantly, these two functions are not mutually exclusive, and both mechanisms presumably contribute to efficient recruitment and turnover of trGTPases on the ribosome. However, conclusive evidence has not been obtained for either case.

Here, we performed single-molecule observations using high-speed atomic force microscopy (HS-AFM) to investigate the structural dynamics of the ribosomal stalk and its binding to trGTPases. HS-AFM clearly visualized the flexible structure of the archaeal P-stalk base on the 50S subunit. Furthermore, we observed that multiple archaeal EF2 (aEF2) molecules were localized around the factor-binding center in the ribosomal P-stalk-dependent manner, and this preferential distribution was similarly observed for archaeal EF1A (aEF1A). These results reveal that the ribosomal stalk recruits the elongation factors to pool around itself while flexibly moving on the ribosome. These mechanistic behaviors are consistent with a factor-pooling mechanism that contributes to efficient binding and action of the elongation factors.

## Results

### Observation of the Ribosomal Stalk on the Large Subunit by HS-AFM.

We first determined the optimal conditions for immobilization of the ribosomes to a mica surface, an atomically flat substrate that makes an ideal sample stage for HS-AFM. The 50S and 30S ribosomal subunits from *E. coli* were gently immobilized on (3-aminopropyl)triethoxysilane-treated mica (AP-mica) (*SI Appendix, Fig. S2 A–E*). In this condition, the heights of the 50S and 30S were estimated to be ~16 and ~12 nm, respectively (*SI Appendix, Fig. S2 F and G*). Given the estimated height of the ribosome, and the fact that AP-mica carries a positive surface charge, it is likely that the ribosomal subunits are immobilized to the stage via their intersubunit rRNA surface which is negatively charged (*SI Appendix, Fig. S2 H and I*). In HS-AFM images of the bacterial 50S ribosomal subunit, a small protrusion that seems to be the L12 stalk base was detected (*SI Appendix, Fig. S2 B and D and Movie S1*). Unfortunately, no further clear images were obtained. Sequence alignments and structural studies show that the archaeal ribosomal P-stalk is larger than that of other kingdoms (*SI Appendix, Fig. S3*). Therefore, we targeted the 50S subunit from a hyperthermophilic archaeon *Pyrococcus furiosus* to investigate the structural dynamics of the ribosomal stalk. We purified the 50S subunit from the archaeal culture, and we succeeded in obtaining a clear HS-AFM image of the 50S subunit which displays three protrusions (Fig. 1A). The structural model of the archaeal 50S subunit and line profile analysis suggest that these three protuberances presumably represent the L1, the central protuberance (CP), and the P-stalk base including the C-terminal part of aP0 (SB), respectively (Fig. 1B).

To confirm whether the protrusion observed in Fig. 1A is the ribosomal P-stalk, we used a hybrid ribosome system that allows removing and reconstitution of the ribosomal stalk in vitro (31). In this system, the bacterial stalk proteins (bL10 and bL12) are removed from the *E. coli* 50S subunit lacking the bacterial ribosomal protein L11 (bL11). The resulting *E. coli* 50S core can be reconstituted by any type of stalk complex and L11. We previously reconstituted the hybrid 50S subunit in which the archaeal ribosomal P-stalk complexes and archaeal L11 (aL11) are introduced into the *E. coli* 50S core and demonstrated that the hybrid 70S ribosome exhibits translation elongation depending on archaeal trGTPases (13, 32, 33). Here, according to the previous report, we

prepared the *E. coli* 50S core and reconstituted the hybrid 50S subunit by adding archaeal aP0•(aP1•aP1)<sub>3</sub> P-stalk complex and aL11. HS-AFM observation of the 50S core alone showed a spherical shape without protrusions (Fig. 1C). On the other hand, similar to Fig. 1A, we succeeded in detecting the protrusions in HS-AFM images of the hybrid 50S subunit (Fig. 1D). These protrusion structures were detected in about 80% of the total hybrid 50S subunits observed (Fig. 1E and *SI Appendix, Fig. S4*). These results reveal that the protrusion observed in Fig. 1A is the ribosomal P-stalk base, and that HS-AFM is useful for the detection and investigation of the ribosomal P-stalk on the 50S ribosomal subunit.

### Structural Dynamics of the Ribosomal P-Stalk on the Large Subunit.

Previous structural studies have shown only part of the ribosomal stalk in the ribosome-bound states. To date, three-dimensional (3D) models of the ribosome containing the ribosomal stalk have been generated by superimposing the crystal structure of the isolated ribosomal stalk onto the ribosome (4, 9). Therefore, our knowledge about the structural dynamics of the ribosomal stalk in the ribosome-bound states is limited. To investigate the structural dynamics of the ribosomal P-stalk on the large subunit, we analyzed HS-AFM images of the archaeal 50S subunit. First, we confirmed that the archaeal ribosomal P-stalk has a canonical state in agreement with previous structural models in which the ribosomal stalk binds to the 23S rRNA through the N-terminal domain of aP0, and the C-terminal side of aP0 is oriented away from the CP (Fig. 2A, *Left*). Intriguingly, an unexpected new state was observed in which the ribosomal P-stalk tip flips toward the CP (Fig. 2A, *Right*). In the HS-AFM movie, the ribosomal P-stalk was moving back and forth between the predicted canonical state and the newly observed flipped state (Fig. 2B and *Movie S2*). To further investigate the structural dynamics of the P-stalk observed in HS-AFM, we performed two kymograph-based analyses. First, we estimated the angle between the proximal and the distal regions of the P-stalk,  $\theta$  (°) using the highest XY coordinates obtained from the cross-sectional line profiles intersecting the three structural features (the center of the ribosome;  $R_{\text{center}}$ , the center of the stalk;  $S_{\text{center}}$ , and the tip of the stalk;  $S_{\text{tip}}$ ) for each HS-AFM image (Fig. 2C–E). The distribution of angle  $\theta$  is plotted (Fig. 2F). We also estimated the flexibility of the P-stalk using an anticorrelation analysis of the two positions as described by Heath et al. (34). The height signals of the P-stalk tip on the canonical and flipped sides of the kymograph obtained from the section line intersecting the P-stalk tip ( $S_{\text{tip}}$ ) were anticorrelated (*SI Appendix, Fig. S5 A and B*). The histograms obtained from the two independent analyses showed two similar peaks, indicating that the ribosomal P-stalk base has, at least, two conformational states (the canonical state and the flipped state) with a ratio of ~60% and ~40%, respectively (Fig. 2F and *SI Appendix, Fig. S5C*). From these time courses (Fig. 2E and *SI Appendix, Fig. S5B*), time constants of the conformational transition from the canonical to the flipped state ( $\tau_c$ ) and the flipped to the canonical state ( $\tau_f$ ) were estimated to be 0.5–0.8 and 0.3–0.5 s, respectively (Fig. 2G and *SI Appendix, Fig. S5D*). The estimated time constants here are in agreement with the ratio of two conformational states. These results showed that the ribosomal P-stalk has a flexible property not only at the C-terminal disordered regions, but also nearer to the stalk base.

### aEF2 Assembles to the Ribosomal P-Stalk on the Large Subunit.

Although the factor-pooling mechanism is hypothesized as one of the functions of the ribosomal stalk, conclusive evidence in support of this mechanism has not been reported. To address this, visualization of the distribution of trGTPases around the ribosome is required at a resolution of nanometer order. HS-AFM can directly visualize the structural dynamics of proteins, including the surrounding environment with nanometer-order

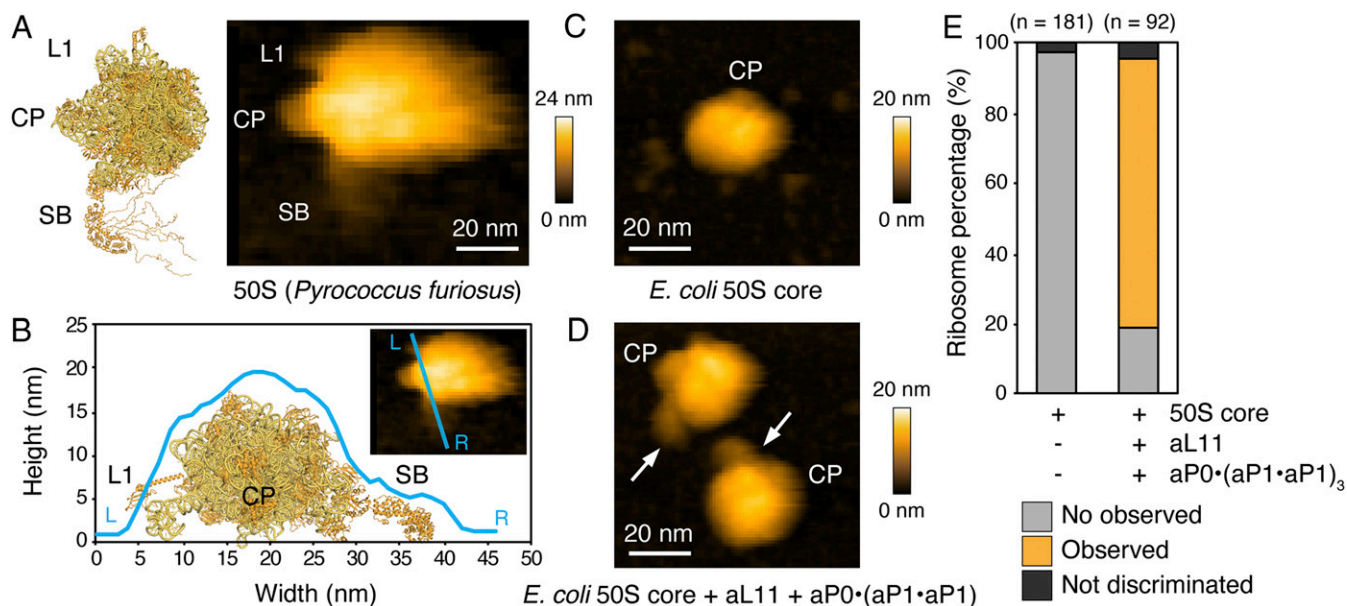


**Fig. 1.** HS-AFM images of the archaeal ribosomal stalk on the 50S ribosomal subunit. (A, Left) A structural docking model of the 50S subunit from *P. furiosus* and the aP0•(aP1•aP1)<sub>3</sub> P-stalk complex made from two coordinates [PDB codes: 3A1Y and 4V6U]. The hinge regions and C-terminal regions of aP0 and aP1 are modeled arbitrarily. (A, Right) A HS-AFM image of the 50S subunit on the AP-mica surface (L1: L1 stalk, CP: central protuberance, SB: P-stalk base). Scan area, 60 × 50 nm with 50 × 40 pixels; scan speed, 150 ms/frame; scale bar, 12 nm. (B) Cross-sectional profile along the cyan line drawn in the HS-AFM image in A. (C and D) HS-AFM images of the 50S core (C) or the hybrid 50S (D) on the AP-mica surface. Scan area, 80 × 80 nm with 80 × 80 pixels; scan speed, 250 ms/frame; scale bar, 20 nm. White arrows indicate the ribosomal P-stalk. (E) Percentage of 50S subunits in which the ribosomal stalk was observed, related to (D) (gray: not observed, orange: observed, and black: not discriminated).

resolution (34–40). We here tested whether the ribosomal P-stalk participates in the formation of a trGTPases factor pool around the ribosome. To this end, we used the hybrid 50S subunit system, which can easily detect the binding of archaeal trGTPases to the ribosomal P-stalk bound to the large ribosomal subunit (13) (SI Appendix, Fig. S6). First, the hybrid 50S subunit was immobilized on the AP-mica surface in the presence of GTP, and aEF2 was added to the sample chamber at 50 nM to give a 10:1 stoichiometry with the ribosome during the HS-AFM observation. After the addition of aEF2, molecules with a size equivalent to aEF2 (~7 nm) appeared on the AP-mica surface (SI Appendix, Fig. S7A). HS-AFM analysis showed that multiple aEF2 molecules gradually assembled to the hybrid 50S subunit (Fig. 3 A and B and SI Appendix, Fig. S7B and Movies S3 and S4). Quantification of aEF2 distribution around the subunit particles revealed that aEF2 molecules preferentially distributed near the ribosomal P-stalk 6.6 fold relative to the opposite control area (Fig. 3 C and D, Upper). The preferential aEF2 distribution was also observed in the presence of guanosine diphosphate (GDP) in which the aEF2 distributed near the ribosomal P-stalk ~4.3 fold relative to the opposite control area (Fig. 3 C and D, Middle). Measuring the distances from the centers of recruited aEF2 molecules to the center of the P-stalk revealed a mean distance of 12.9 nm for aEF2•GTP and 11.5 nm for aEF2•GDP, respectively (Fig. 3 E, Upper and Middle). To investigate whether the preferential aEF2 distribution was dependent on the ribosomal P-stalk, we performed HS-AFM observation using the *E. coli* 50S core instead of the hybrid 50S subunit. As a result, an unbiased even distribution of aEF2 was observed (Fig. 3 C–E, Lower and SI Appendix, Fig. S7C). These results demonstrate that the ribosomal P-stalk recruits multiple aEF2 molecules around itself for increasing the local concentration of aEF2 in a manner consistent with the factor-pooling hypothesis.

#### The Ribosomal P-Stalk Simultaneously Binds to Multiple aEF2 Molecules.

The archaeal ribosomal P-stalk has seven copies of the C-terminal region, which presumably bind to trGTPase individually (8, 9). Nomura et al. previously observed that the isolated archaeal ribosomal P-stalk simultaneously binds to, at least, three aEF2 molecules by ultracentrifugation experiments (13). However, the maximum number of aEF2 molecules that can be simultaneously bound to the ribosomal P-stalk is unclear. To examine this question, we preincubated hybrid 50S subunits with various concentrations of aEF2 in the presence of GTP and immobilized them on AP-mica. After washing, aEF2 molecules bound to the ribosomal P-stalk were counted. Unfortunately, when the aEF2 concentration was higher than 80 nM, it became difficult to distinguish between aEF2 bound to the ribosomal P-stalk and free aEF2 on the AP-mica during HS-AFM observation. Therefore, we observed in the range of 5–75 nM of aEF2, and we counted more than 100 50S particles at each concentration. The number of aEF2 molecules bound around to the ribosomal P-stalk increased in a concentration-dependent manner, and up to seven aEF2 molecules simultaneously bound to the ribosomal P-stalk (Fig. 4 A and B). The results reveal that each P-stalk C-terminal region can independently recruit an aEF2 molecule, and the number of recruited aEF2 molecules depends on the concentration of aEF2.

#### aEF1A Assembles to the Ribosomal P-Stalk Both in GTP- and GDP-Bound Forms.

Efficient binding and dissociation of the EF1A•GTP•aa-tRNA ternary complex to the ribosome are critical for correct codon reading at the A-site and for improving translation accuracy. In previous studies, we have demonstrated that the ribosomal P-stalk is also involved in the recruitment of EF1A•GTP•aa-tRNA and the activation of GTP hydrolysis (33, 41). We next visualized the binding of aEF1A to the ribosomal P-stalk on the large subunit. Using HS-AFM, we observed that aEF1A (~5 nm) transiently interacts with the ribosomal P-stalk on the 50S subunit in the presence of GTP (Fig. 5 A and SI Appendix, Fig. S8 A and B

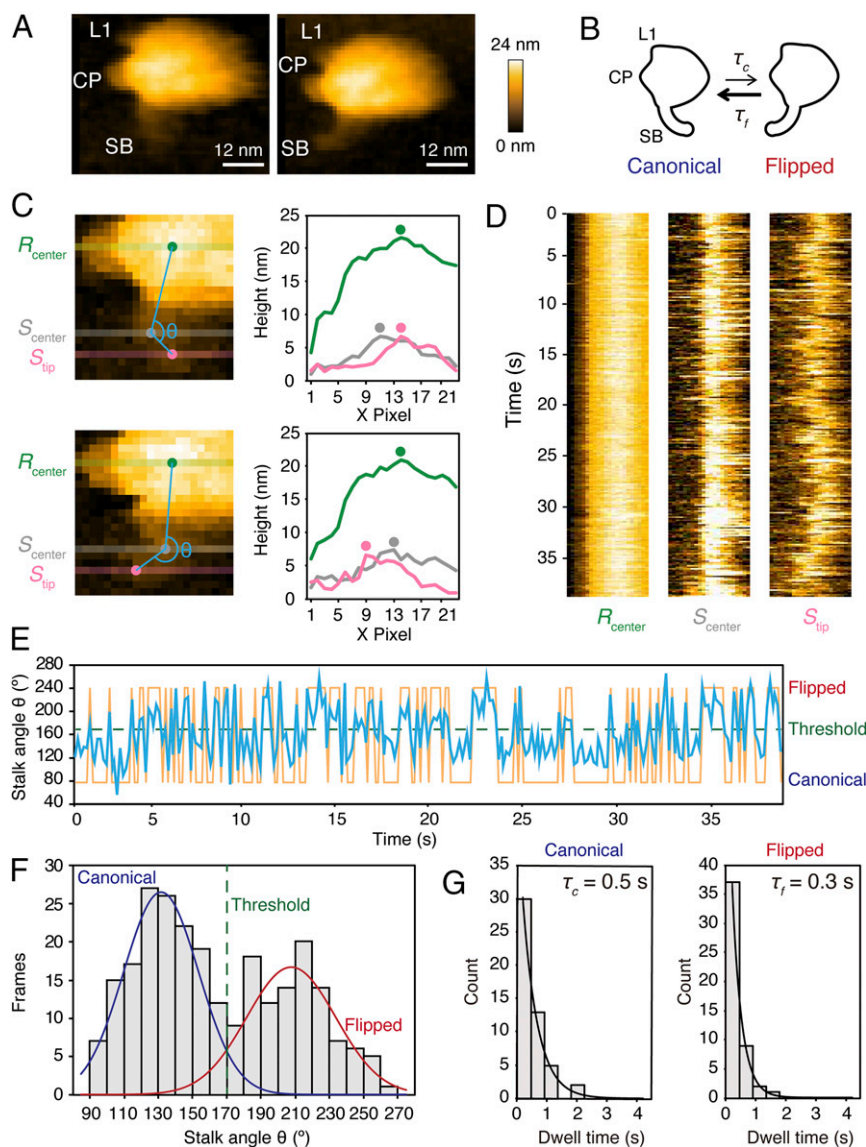


**Fig. 2.** Structural dynamics of the ribosomal P-stalk base on the archaeal 50S subunit. (A) HS-AFM images of the ribosomal stalk base in the canonical (Left) and flipped (Right) states (L1: L1 stalk, CP: central protuberance, SB: P-stalk base). Scan area,  $60 \times 50$  nm with  $50 \times 40$  pixels; scan speed, 150 ms/frame; scale bar, 12 nm. (B) Schematics of two conformational states of the ribosomal P-stalk base, related to (A). (C) Cross-sectional profiles (Right) along the green line (ribosome center:  $R_{center}$ ), gray line (stalk center:  $S_{center}$ ), and pink line (stalk tip:  $S_{tip}$ ) drawn in the HS-AFM images (Left). The highest points (represented as dots) in the cross-sectional profiles were connected, and the angles between the proximal and the distal regions of the P-stalk were estimated. The angles between the proximal and the distal regions of the stalk are indicated by the cyan line ( $\theta$ ) in the left two images. (D) Kymographs across the green line ( $R_{center}$ ), gray line ( $S_{center}$ ), and pink line ( $S_{tip}$ ) drawn in the HS-AFM images in (C) at 1 pixel per line. (E) Time course of the stalk base angle ( $\theta$ ), related to (C) and [Movie S2](#), and fitted with a two-state model (orange trace). Threshold was obtained from (F). (F) Histogram of the stalk base angles  $\theta$ . (G) Dwell times in the canonical and flipped states of the P-stalk estimated by the angle analysis. Each black line overlaid on the corresponding histogram of the dwell time was obtained by fitting the histogram to a first order reaction model with the time constants ( $\tau_c$  and  $\tau_f$ ) shown.

and [Movie S5](#)). In this condition, aEF1A molecules associated near the ribosomal P-stalk 4.2 fold more often relative to the opposite control area, forming a pool of aEF1A (Fig. 5 B and C, Upper), and the histogram of distances from the center of each aEF1A molecule to the center of the P-stalk showed a mean distance of 9.5 nm for the P-stalk-bound aEF1A (Fig. 5 D, Upper). The preferential distribution of aEF1A•GTP was not observed using the 50S core (Fig. 5 B–D, Lower). Therefore, similar to aEF2, aEF1A localizes near the factor-binding center in a ribosomal P-stalk-dependent manner. The binding and dissociation of aEF1A•GTP to the ribosomal P-stalk ([Movies S5](#) and [S6](#)) seems to take place more rapidly than aEF2•GTP ([Movie S4](#)). The short-binding lifetime of aEF1A•GTP to the ribosomal P-stalk

may reflect the necessity for kinetically rapid association and dissociation to allow efficient codon–anticodon reading tests.

It has been demonstrated that the conformation of the GDP-bound form of aEF1A and its binding mode to the C-terminal region of the aP1 stalk are somewhat different from those of the GTP-bound form (41, 42). We, thus, analyzed the binding of aEF1A•GDP to the ribosomal P-stalk on the large subunit. The results also showed the preferential distribution of aEF1A•GDP in proximity to the P-stalk, revealing that both GTP- and GDP-binding forms of aEF1A localize around the factor-binding center of the ribosome (Fig. 5 E, Upper). The aEF1A•GDP associated near the ribosomal P-stalk 2.6 fold more often relative to the opposite control area (Fig. 5 F and G, Upper). These GTP- and

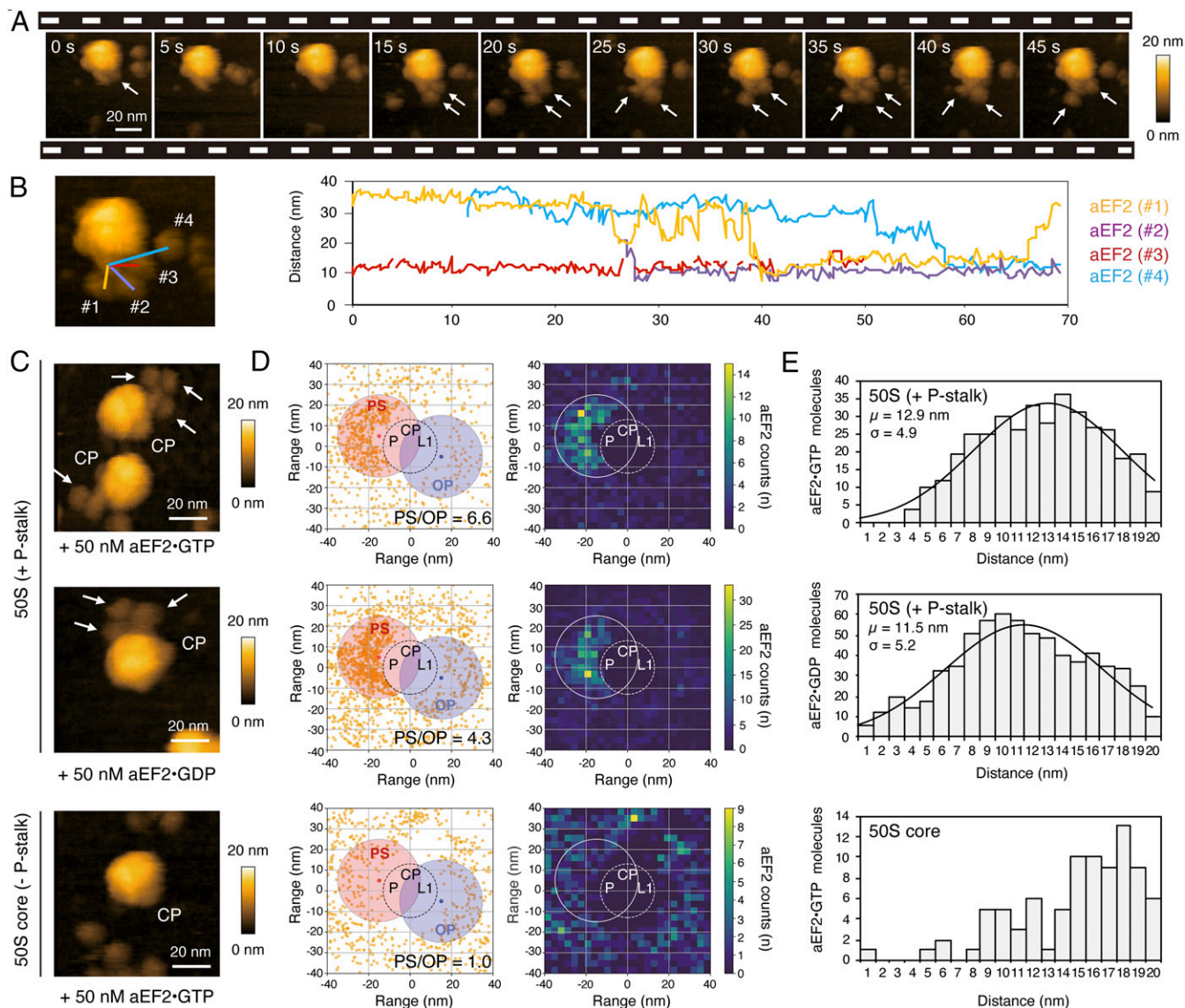


**Fig. 3.** The ribosomal stalk simultaneously recruits multiple aEF2•GTP to the ribosome to form the factor pool. (A) Sequential HS-AFM images of the hybrid 50S subunit after the addition of aEF2•GTP on the AP-mica surface. aEF2•GTP molecules bound to the ribosomal stalk are indicated by white arrows. Scan area,  $80 \times 80$  nm with  $90 \times 90$  pixels; scan speed, 250 ms/frame; scale bar, 20 nm. (B) A HS-AFM image (Left) and time courses (Right) of the distance between the ribosomal P-stalk and individual aEF2•GTP molecules (no. 1: orange, no. 2: purple, no. 3: red, and no. 4: cyan) related to (A). (C) Typical HS-AFM images of the hybrid 50S in the presence of 50 nM aEF2•GTP (Top), the hybrid 50S in the presence of 50 nM aEF2•GDP (Middle), and the 50S core in the presence of 50 nM aEF2•GTP (Bottom). Scan area,  $80 \times 80$  nm with  $90 \times 90$  pixels; scan speed, 250 ms/frame; scale bar, 20 nm. aEF2 molecules bound to the ribosomal stalk are indicated by white arrows. (D) Dot plots (Left) and heat maps (Right) of aEF2•GTP molecules around the hybrid 50S subunit (top); 930 aEF2 molecules and 156 subunits were analyzed, aEF2•GDP molecules around the hybrid 50S subunit (middle); 1,609 aEF2 molecules and 245 subunits were analyzed, and aEF2•GTP molecules around the 50S core (bottom); 1,316 aEF2 molecules and 112 subunits were analyzed, related to Fig. 3C. The area near the P-stalk side (PS; radius, 20 nm) or the area opposite the P-stalk (OP; radius, 20 nm) are represented by red and blue circles, respectively. The ratios of the number of molecules of aEF2 (PS/OP) are 6.6, 4.3, and 1.0, respectively. Dotted circles approximately represent the 50S subunit (L1: L1 stalk, CP: central protuberance, P: P-stalk). (E) Histograms of the distances between the center of the P-stalk side (PS) and each aEF2 molecules, related to (D). The mean ( $\mu$ ) and SD ( $\sigma$ ) fitted by Gaussians are 12.9 and 4.9 nm (Top), respectively, and 11.5 and 5.2 nm (Middle), respectively.

GDP-dependent factor-pool formations are consistent with a similar binding affinity of aP1 to aEF1A•GTP and aEF1A•GDP (41, 42) (SI Appendix, Table S1). Since the formation of the aEF1A pooling was not observed in nucleotide-free conditions, the present HS-AFM data show that aEF1A assembly is dependent on GTP and GDP (Fig. 5 E–G, Lower and SI Appendix, Fig. S8C). Taken together, these results indicate that the ribosomal P-stalk increases the local concentration of aEF1A near the factor-binding center, in agreement with the factor-pooling hypothesis to efficient decoding by EF1A•GTP•aa-tRNA and translation elongation.

## Discussion

In this study, using HS-AFM, we directly visualized: 1) the structural dynamics of the archaeal ribosomal P-stalk on the 50S subunit, 2) the assembly processes of trGTPases to the ribosomal P-stalk, and 3) the P-stalk-dependent preferential distribution of trGTPases around the factor-binding center. These results reveal that the ribosomal P-stalk forms a trGTPase pool near the factor-binding center for efficient trGTPases turnovers. It must be noted that the trGTPases factor pool observed in this study was formed on the hybrid 50S subunit immobilized on AP-mica, therefore, we did not directly visualize the full biological

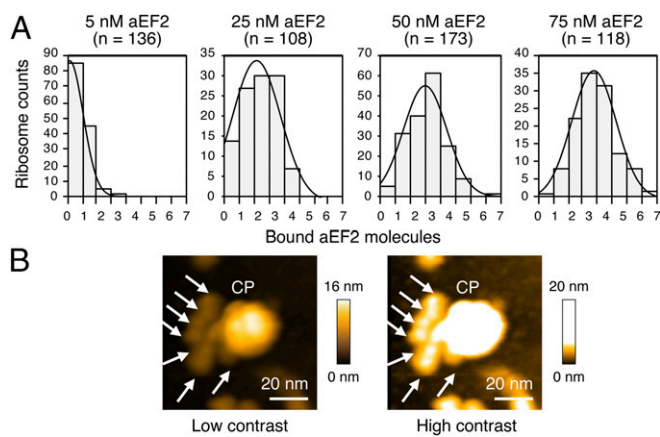


**Fig. 4.** The ribosomal stalk simultaneously binds to multiple aEF2 molecules in a concentration-dependent manner. (A) Histograms of the binding numbers of aEF2 to the ribosomal stalk. The hybrid 50S subunits (5 nM) were incubated with various concentrations of aEF2•GTP (5, 25, 50, and 75 nM) and immobilized to the AP-mica surface. After washing, the number of aEF2 molecules bound to each ribosomal stalk was counted by HS-AFM ( $n$ : number of 50S particles counted). (B) HS-AFM images of the hybrid 50S bound to seven aEF2 molecules with low (Left) and high (Right) contrasts. Scan area,  $80 \times 80$  nm with  $90 \times 90$  pixels; scan speed, 250 ms/frame; scale bar, 20 nm. aEF2 molecules bound to the ribosomal stalk are indicated by white arrows.

translation processes mediated by the 70S ribosome and other cofactors. However, the 30S subunit does not influence the interactions between the ribosomal P-stalk and the trGTPases, and the hybrid system we used accurately recapitulates the functional role of the archaeal and eukaryotic ribosomal P-stalks in translation elongation (10, 31–33, 41). Therefore, we believe that the formation of the trGTPase factor pool we observed here presumably reflects the actual translation elongation status is likely to occur during actual biological translation elongation.

Using HS-AFM, we observed an unexpected structural flexibility of the ribosomal P-stalk base on the ribosome (Fig. 2 and *SI Appendix*, Fig. S5). This structural rearrangement of the P-stalk base has not been detected in X-ray crystallography and cryo-EM studies of ribosomal particles. Our present study demonstrates that the structural rearrangements of the ribosomal P-stalk base take place with the time constants  $\tau_c$  (0.5–0.8 s) and  $\tau_f$  (0.3–0.5 s). Since these structural rearrangements might be slowed down by the interaction with the AP-mica surface, the P-stalk presumably moves more rapidly in solution. We hypothesize that the unexpected frequent rearrangements of the P-stalk play some functional role. A reasonable hypothesis is that the movement of the P-stalk base expands the range of movement of the C-terminal part of each stalk protein, resulting in increased frequency of the stalk interaction with translation factors around the ribosome (14).

The increases in the local concentration of aEF2/aEF1A depends on the presence of the ribosomal P-stalk, suggesting that the P-stalk works as the factor-pooling platform. We hypothesize that this mechanism is driven by two key properties of the P-stalk: The rapid flipping movement we described above, and the presence of multiple copies of the flexible C-terminal region for parallel binding of trGTPases. HS-AFM analysis showed the mean distances from the center of the P-stalk base to the center of each trGTPase were 12.9 nm for aEF2•GTP and 9.5 nm for aEF1A•GTP, respectively (Figs. 3E and 5D). These observations are consistent with the fact that the C-terminal regions of eukaryotic P1/P2, which is homologous to aP1, can extend up to  $\sim 12.5$  nm away from its N-terminal dimerization domain (14). The number of C-terminal regions of the ribosomal stalk is correlated to the trGTPase activity, polypeptide elongation rate in vitro (9, 13, 33, 43), and translation fidelity in vivo (44). From

these lines of evidence, we infer that the ribosomal stalk participates in forming a pool of different EF1A•GTP•aa-tRNA ternary complexes around the P-stalk for efficient codon-anticodon reading tests and that maintaining this aEF1A/aEF2 pool is important for rapid and accurate translation elongation in crowded intracellular environments (Fig. 6).

Recently, using the single-molecule fluorescence method, Mustafi et al. tracked a single molecule of EF-Tu fused with the fluorescent protein mEos2 in *E. coli* cells with resolution on the micrometer order and classified EF-Tu into two groups based on differences in their diffusion rates (45). In their observations, EF-Tu with a slow diffusion rate ( $\sim 60\%$  of the total EF-Tu) was colocalized with the ribosome in a manner dependent on interaction with the L12 stalk, and the average stoichiometry of EF-Tu binding to the ribosome was estimated to be 3.5 molecules of EF-Tu per ribosome. Although it is unknown whether EF-Tu has a preferential distribution around the factor-binding center based on these experiments, their study is consistent with our present observations and suggests that the factor-pooling mechanism visualized by HS-AFM is biologically relevant.

In translation initiation, the ribosomal stalk interacts with the GTPase initiation factor IF2 (aIF5B in archaea and eIF5B in eukaryotes) to promote large and small subunit joining and selectivity for the initiation AUG codon (46, 47). The ribosomal stalk also plays a functional role in the recruitment of ribosome recycling factor ABCE1 and its ATP hydrolysis in archaea and eukaryotes (48). Point mutations disrupting the binding of the ribosomal stalk to eIF5B and ABCE1 inhibit cell viability, suggesting that the ribosomal stalk maintains these functional interactions with eIF5B and ABCE1 in vivo (47, 48). Therefore, at least, four translation factors appear to compete with each other as the binding partners for the ribosomal stalk. The binding affinity of the C-terminal region of the stalk to each translation factor does not differ significantly (*SI Appendix*, Table S1) (42, 47–49). Given that the number of translation factors bound around the ribosomal stalk is concentration dependent (Fig. 4), it is likely that the identities and numbers of factors that bind to the multiple stalk C-terminal regions depend on the local concentration of each factor. Supporting this notion is the fact that EF1A, which is the most likely trGTPase to interact with the ribosome in translation, is one of the most abundant proteins in the cell.

Unfortunately, our HS-AFM analyses do not provide any information about the action of the ribosomal stalk and trGTPases once bound to the factor-binding center of the ribosome. Previous study reported that the stalk may have the ability to stabilize the GTP-bound trGTPases on the factor-binding center via interaction of the stalk with ribosomal protein uL11, possibly promoting trGTPases-dependent polypeptide synthesis and/or GTPase activation (50). The stalk also participates in the release of inorganic phosphate from EF-G after GTP hydrolysis (3). Therefore, it is expected that the stalk has, at least, a two-step independent function: the binding of trGTPase to the factor-binding center by forming the factor pool and promoting GTP hydrolysis by factor stabilizing at the factor-binding center. Furthermore, HS-AFM clearly showed that each copy of aP0 and aP1 also has the ability to interact with aEF1A•GDP or aEF2•GDP molecules, suggesting that the ribosomal P-stalk keeps its aEF1A/aEF2 pool bound nearby even after their dissociation from the ribosomal factor-binding center after GTP hydrolysis. The retention of the aEF1A•GDP/aEF2•GDP pool may also allow rapid reuse of trGTPases after nucleotide exchange reaction. Therefore, it seems likely that, by making and maintaining the aEF1A/aEF2 pool, the stalk efficiently promotes not only the recruitment of GTP-bound trGTPases to the factor-binding center and their actions including GTP hydrolysis on the ribosome, but also the retention of GDP-bound trGTPases after their dissociation from the ribosomal factor-binding center.

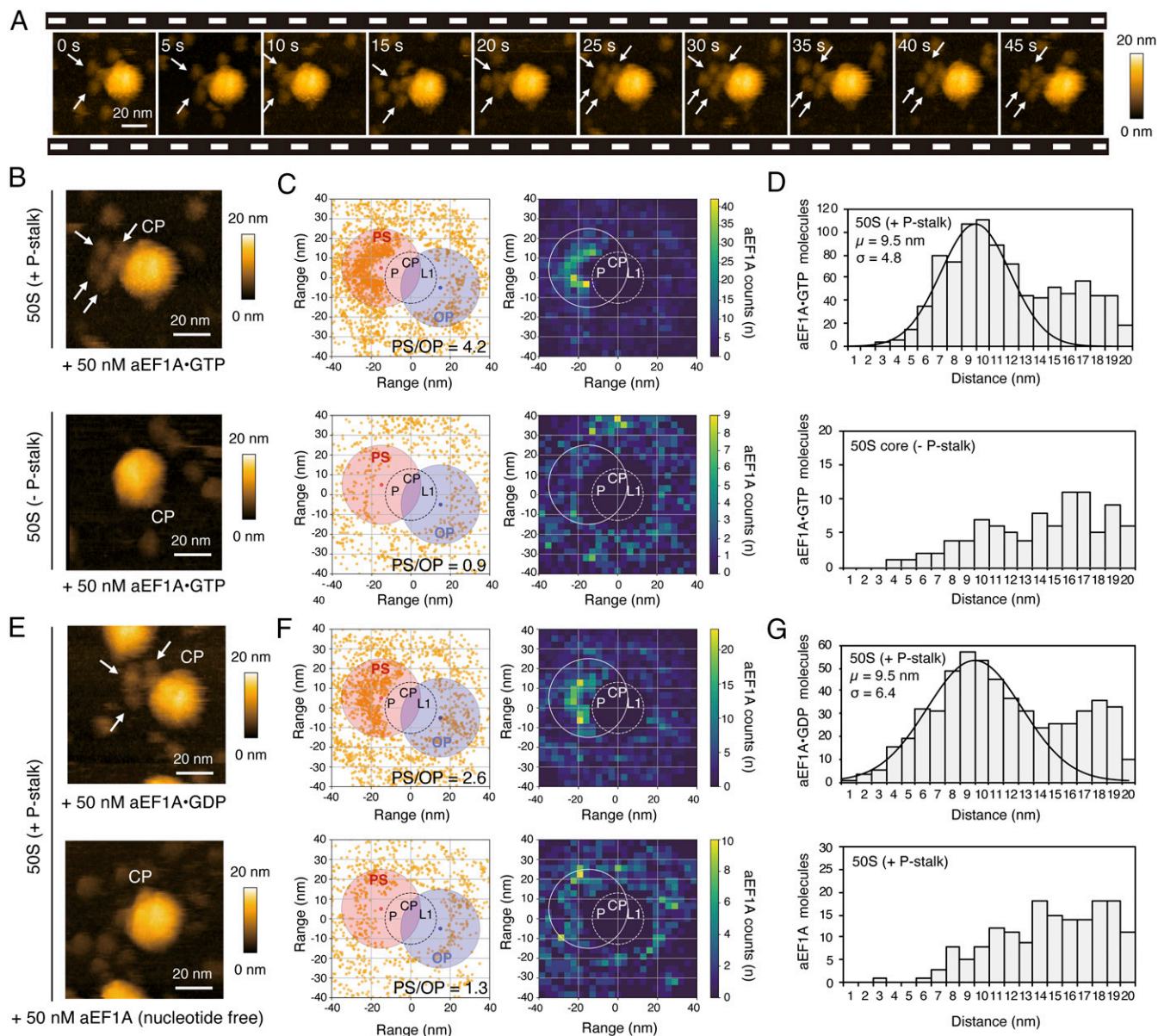


**Fig. 5.** Preferential distribution of aEF1A around the 50S subunit dependent on the ribosomal stalk. (A) Sequential HS-AFM images of the hybrid 50S subunit in the presence of 50 nM aEF1A•GTP on the AP-mica surface. aEF1A•GTP molecules bound to the ribosomal stalk are indicated by white arrows. Scan area,  $80 \times 80$  nm with  $90 \times 90$  pixels; scan speed, 250 ms/frame; scale bar, 20 nm. (B) Typical HS-AFM images of the hybrid 50S (above) or 50S core (below) in the presence of 50 nM aEF1A•GTP. Scan area,  $80 \times 80$  nm with  $90 \times 90$  pixels; scan speed, 250 ms/frame; scale bar, 20 nm. aEF1A•GTP molecules bound to the ribosomal stalk are indicated by white arrows. (C) Dot plots (Left) and heat maps (Right) of aEF1A•GTP molecules around the hybrid 50S subunit (above: 2,490 aEF1A molecules and 278 subunits were analyzed) and aEF1A•GTP molecules around the 50S core (below: 937 aEF1A molecules and 141 subunits were analyzed). Dotted circles approximately represent the 50S subunit (L1: L1 stalk, CP: central protuberance, P: P-stalk). The area near the PS (radius, 20 nm) or the area OP (radius, 20 nm) are represented by red and blue circles, respectively. The ratios of the number of molecules of aEF1A (PS/OP) are 4.2 (above) and 0.9 (below), respectively. (D) Histograms of the distances between the center of the area near the PS and each aEF1A•GTP molecules, related to (C). The mean ( $\mu$ ) and SD ( $\sigma$ ) fitted by Gaussians are 9.5 and 4.8 nm, respectively (above). (E) Typical HS-AFM images of the hybrid 50S in the presence of 50 nM aEF1A•GDP (above) or nucleotide-free aEF1A (below). Scan area,  $80 \times 80$  nm with  $90 \times 90$  pixels; scan speed, 250 ms/frame; scale bar, 20 nm. aEF1A•GTP molecules bound to the ribosomal stalk are indicated by white arrows. (F) Dot plots (Left) and heat maps (Right) of aEF1A•GDP molecules (above: 1,912 aEF1A molecules and 211 subunits were analyzed) and nucleotide-free aEF1A molecules (below: 1,088 aEF1A molecules and 89 subunits were analyzed) around the hybrid 50S subunit. The ratios of the number of molecules of aEF1A (PS/OP) are 2.6 (above) and 1.3 (below), respectively. (G) Histograms of the distances between the center of the area near the PS and each aEF1A molecule, related to (E). The mean ( $\mu$ ) and SD ( $\sigma$ ) fitted by Gaussians are 9.5 and 6.4 nm, respectively (above).

In conclusion, this study provides visual evidence for the trGTPase factor-pooling mechanism by the ribosomal P-stalk. Translation is a collection of dynamic processes in which the ribosome undergoes sequential conformational changes and interacts with many accessory factors. Since HS-AFM has advantages in observation of not only structural dynamics, but also spatial distributions of biomolecules, future work with HS-AFM will

provide further important information to understand the dynamic behaviors of these complex translational machineries.

## Materials and Methods

**Sample Preparation.** The plasmids for expression of *Pyrococcus horikoshii* aP0, aP1, and aL11 were constructed, and the proteins were expressed and purified as described previously (9, 32). The plasmids for expression of

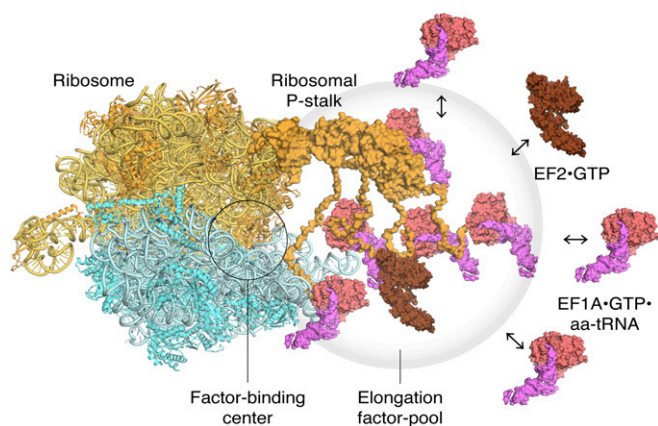


**Fig. 6.** Model of translating ribosomes and elongation factors. EF1A•GTP•aa-tRNA and EF2 assemble to the ribosomal stalk on the translating ribosome. The translation factor pool contributes to efficient protein synthesis in a crowded intracellular environment.

*P. furiosus* aEF2 and aEF1A were constructed, and the proteins were expressed using an *E. coli* expression system and isolated as described previously (33, 41). The prepared aEF1A sample contained tightly bound GDP (41). In order to observe the dynamics of GTP-bound aEF1A binding to the ribosomes, we prepared a nucleotide-free aEF1A by bacterial alkaline phosphatase treatment (51). The 50S ribosomal subunits from *P. furiosus* were prepared as described previously (13). The 50S and 30S ribosomal subunits from the *E. coli* Q13 strain and the 50S subunit lacking bL11 from the *E. coli* AM68 strain were prepared as described previously (31, 52). The *E. coli* 50S core was prepared as described previously (31). The hybrid 50S subunits were reconstituted by mixing the *E. coli* 50S core with purified archaeal aL11 protein and purified aP0•(aP1•aP1)<sub>3</sub> complexes as described previously (32). In brief, 50S cores (10 pmol) were incubated with aL11 (20 pmol) and aP0•(aP1•aP1)<sub>3</sub> complex (20 pmol) in 10  $\mu$ L of buffer A (20 mM 2-amino-2-hydroxymethyl-1,3-propanediol (Tris)-HCl, pH 7.6, 10 mM MgCl<sub>2</sub>, and 50 mM NH<sub>4</sub>Cl) for 10 min at 37  $^{\circ}$ C.

**Native Polyacrylamide Gel Electrophoresis.** The 50S cores or hybrid 50S subunits (5 pmol) were incubated without or with aEF2 (5, 10, 15, 20, 25, 30, 35, 40, and 45 pmol) in 10  $\mu$ L of buffer A for 10 min at 37  $^{\circ}$ C. After incubation, 0.7  $\mu$ L of loading buffer with dye (50% [vol/vol] glycerol, 0.1% [wt/vol] bromophenol blue, 0.1% [wt/vol] xylene cyanol) was added. The total sample solution was subjected to acrylamide-agarose composite gel electrophoresis as described previously (10).

**HS-AFM Observations.** A laboratory-built tapping mode HS-AFM was used (53, 54). The short cantilevers used (BL-AC10DS-A2) were purchased from Olympus. The spring constant of the cantilever was  $\sim$ 100 pN/nm. The resonant frequency and the quality factor of the cantilever in liquid were  $\sim$ 500 kHz and  $\sim$ 1.5, respectively. An amorphous carbon tip was fabricated on the original AFM tip by electron beam deposition. The length of the additional AFM tip was  $\sim$ 500 nm, and the radius of the apex of the tip was  $\sim$ 4 nm. The free oscillation amplitude of the cantilever was 2 nm, and the set-point amplitude was set to 90% of the free amplitude.

For HS-AFM observations of the 50S subunits, a mica surface was treated for 5 min with 0.01% (vol/vol) (3-aminopropyl)triethoxysilane (Sigma-Aldrich). HS-AFM observations of the 50S subunits from *P. furiosus* or preassembled hybrid 50S subunits were performed as follows. The ribosome mixture containing *P.*

*furiosus* 50S (5 nM) or the hybrid 50S (5 nM) subunits was incubated in buffer A for 10 min at 37  $^{\circ}$ C. The ribosome mixture (2  $\mu$ L) was placed on the AP-mica and incubated for 5 min at room temperature. After washing with 20  $\mu$ L of buffer A, the stage was immersed in 60  $\mu$ L of buffer A filled in the liquid cell of the cantilever holder, and HS-AFM observation was started.

Observation of aEF2 binding to hybrid 50S subunits was performed as follows. While observing the hybrid 50S subunits under the conditions described above, aEF2 and GTP were added to the liquid cell at final concentrations of 50 and 1 mM, respectively. After adding aEF2 and GTP, HS-AFM observation was started immediately.

Counting of the ribosomal stalk-bound aEF2 was performed as follows. The mixture containing the hybrid 50S subunits (5 nM) and aEF2 (5, 25, 50, and 75 nM) was incubated in buffer A containing 1 mM GTP for 10 min at 37  $^{\circ}$ C. This ribosome mixture (2  $\mu$ L) was placed on the AP-mica and incubated for 5 min at room temperature. After washing with 20  $\mu$ L of buffer A, the stage was immersed in 60  $\mu$ L of buffer A in the liquid cell of the cantilever holder, and HS-AFM observation was started.

The observation of aEF1A was performed as follows. The mixture containing the hybrid 50S subunits (5 nM) and aEF1A (50 nM) was incubated in buffer A in the presence or absence of 1 mM GTP or GDP for 10 min at 37  $^{\circ}$ C. This ribosome mixture (2  $\mu$ L) was placed on the AP-mica and incubated for 5 min at room temperature. After washing with 20  $\mu$ L of buffer A, the stage was immersed in 60  $\mu$ L of buffer A, and HS-AFM observation was started.

**Analyzing of HS-AFM Images.** HS-AFM images were viewed and analyzed using a laboratory-built software, Kodec4.5.7.39 (55). A flattening filter to make the XY plane flat was applied to individual images. The heights of ribosomal subunits were determined using a cross-sectional analysis. Angles of the ribosomal P-stalk base were estimated as follows. Initially, the HS-AFM movies were drift corrected by a laboratory-built software, Falcon Viewer (56). Three cross-sectional profiles at 1 pixel per line intersecting the center of the 50S ribosome ( $R_{center}$ ), the center of the P-stalk ( $S_{center}$ ), and the tip of the P-stalk ( $S_{tip}$ ), respectively, were obtained from individual HS-AFM images by which kymographs were assembled by ImageJ as described previously (57). For the angle analysis, the highest points were obtained from each cross-sectional profile as XY coordinates, and the stalk base angles  $\theta$  among three coordinates were calculated for each image. The anticorrelation analysis was performed using only the section profile intersecting the tip of the P-stalk ( $S_{tip}$ ). The height signals of the P-stalk on the canonical and flipped sides were determined from the average height of the three pixels for each side.

The distributions of aEF2 and aEF1A were quantified as follows. First, the XY coordinates of the center of the ribosome (CR), the central protuberance (CP), and the center of the translational factors (CT) were manually obtained from individual HS-AFM images. For each frame, all coordinates were translated so that the CR was placed on the origin, and all coordinates were rotated so that the CP was placed on the positive y axis. Then, the CT values from all images were plotted as XY coordinates which were used to create a heat map showing the distribution of the translation factors.

**Data Availability.** All study data are included in the article, supporting information, and Protein Data Bank (PDB) (PDB codes: 3A1Y and 4V6U).

**ACKNOWLEDGMENTS.** We thank Dr. Steven J. McArthur for critical reading and the English language improvement of the paper; Dr. Kosuke Ito for many discussions; Dr. Yoshizumi Ishino and Dr. Sonoko Ishino for kindly providing the culture pellets of *P. furiosus*; Ms. Aimi Makino, Dr. Toshio Ando, Dr. Takayuki Uchihashi, and Dr. Takahiro Watanabe-Nakayama for the technical support of the HS-AFM. This work was supported by grants from JSPS (20J00036 to H.I., 19H03155 to T.U., and 20H00327 to N.K.) and a grant from JST-CREST (JPMJCR1762 to N.K.). This work was also supported, in part, by Bio-SPMs collaborative research of WPI-NanoLSI, Kanazawa University.

1. M. V. Rodnina, W. Wintermeyer, Recent mechanistic insights into eukaryotic ribosomes. *Curr. Opin. Cell Biol.* **21**, 435–443 (2009).
2. T. M. Schmeing, V. Ramakrishnan, What recent ribosome structures have revealed about the mechanism of translation. *Nature* **461**, 1234–1242 (2009).
3. D. Mohr, W. Wintermeyer, M. V. Rodnina, GTPase activation of elongation factors Tu and G on the ribosome. *Biochemistry* **41**, 12520–12528 (2002).
4. M. Diaconu et al., Structural basis for the function of the ribosomal L7/12 stalk in factor binding and GTPase activation. *Cell* **121**, 991–1004 (2005).
5. A. Liljas, S. Sanyal, The enigmatic ribosomal stalk. *Q. Rev. Biophys.* **51**, e12 (2018).
6. M. V. Rodnina, T. Pape, R. Fricke, L. Kuhn, W. Wintermeyer, Initial binding of the elongation factor Tu•GTP•aminoacyl-tRNA complex preceding codon recognition on the ribosome. *J. Biol. Chem.* **271**, 646–652 (1996).

7. A. Savelsbergh et al., An elongation factor G-induced ribosome rearrangement precedes tRNA-mRNA translocation. *Mol. Cell* **11**, 1517–1523 (2003).
8. Y. Maki et al., Three binding sites for stalk protein dimers are generally present in ribosomes from archaeal organism. *J. Biol. Chem.* **282**, 32827–32833 (2007).
9. T. Naganuma et al., Structural basis for translation factor recruitment to the eukaryotic/archaeal ribosomes. *J. Biol. Chem.* **285**, 4747–4756 (2010).
10. A. Hagiya et al., A mode of assembly of P0, P1, and P2 proteins at the GTPase-associated center in animal ribosome: In vitro analyses with P0 truncation mutants. *J. Biol. Chem.* **280**, 39193–39199 (2005).
11. E. V. Bocharov et al., From structure and dynamics of protein L7/L12 to molecular switching in ribosome. *J. Biol. Chem.* **279**, 17697–17706 (2004).

12. M. Helgstrand *et al.*, The ribosomal stalk binds to translation factors IF2, EF-Tu, EF-G and RF3 via a conserved region of the L12 C-terminal domain. *J. Mol. Biol.* **365**, 468–479 (2007).
13. N. Nomura *et al.*, Archaeal ribosomal stalk protein interacts with translation factors in a nucleotide-independent manner via its conserved C terminus. *Proc. Natl. Acad. Sci. U.S.A.* **109**, 3748–3753 (2012).
14. K.-M. Lee *et al.*, Solution structure of human P1•P2 heterodimer provides insights into the role of eukaryotic stalk in recruiting the ribosome-inactivating protein trichostatin to the ribosome. *Nucleic Acids Res.* **41**, 8776–8787 (2013).
15. P. Grela *et al.*, Structural relationships among the ribosomal stalk proteins from the three domains of life. *J. Mol. Evol.* **67**, 154–167 (2008).
16. J. A. Lake, Ribosome structure determined by electron microscopy of *Escherichia coli* small subunits, large subunits and monomeric ribosomes. *J. Mol. Biol.* **105**, 131–139 (1976).
17. M. Boublik, W. Hellmann, H. E. Roth, Localization of ribosomal proteins L7/L12 in the 50 S subunit of *Escherichia coli* Ribosomes by electron microscopy. *J. Mol. Biol.* **107**, 479–490 (1976).
18. W. A. Strycharz, M. Nomura, J. A. Lake, Ribosomal proteins L7/L12 localized at a single region of the large subunit by immune electron microscopy. *J. Mol. Biol.* **126**, 123–140 (1978).
19. T. M. Schmeing *et al.*, The crystal structure of the ribosome bound to EF-Tu and aminoacyl-tRNA. *Science* **326**, 688–694 (2009).
20. R. M. Voorhees, T. M. Schmeing, A. C. Kelley, V. Ramakrishnan, The mechanism for activation of GTP hydrolysis on the ribosome. *Science* **330**, 835–838 (2010).
21. J. Lin, M. G. Gagnon, D. Bulkley, T. A. Steitz, Conformational changes of elongation factor G on the ribosome during tRNA translocation. *Cell* **160**, 219–227 (2015).
22. H. Khatler, A. G. Myasnikov, S. K. Natchiar, B. P. Klaholz, Structure of the human 80S ribosome. *Nature* **520**, 640–645 (2015).
23. X. Wang *et al.*, Probing the dynamic stalk region of the ribosome using solution NMR. *Sci. Rep.* **9**, 13528 (2019).
24. H. Stark *et al.*, Visualization of elongation factor Tu on the *Escherichia coli* ribosome. *Nature* **389**, 403–406 (1997).
25. P. P. Datta, M. R. Sharma, L. Qi, J. Frank, R. K. Agrawal, Interaction of the G' domain of elongation factor G and the C-terminal domain of ribosomal protein L7/L12 during translocation as revealed by cryo-EM. *Mol. Cell* **20**, 723–731 (2005).
26. S. R. Connell *et al.*, Structural basis for interaction of the ribosome with the switch regions of GTP-bound elongation factors. *Mol. Cell* **25**, 751–764 (2007).
27. J. M. Harms *et al.*, Translational regulation via L11: Molecular switches on the ribosome turned on and off by thiostrepton and micrococin. *Mol. Cell* **30**, 26–38 (2008).
28. Y.-G. Gao *et al.*, The structure of the ribosome with elongation factor G trapped in the posttranslocational state. *Science* **326**, 694–699 (2009).
29. Y. Chen, S. Feng, V. Kumar, R. Ero, Y.-G. Gao, Structure of EF-G-ribosome complex in a pretranslocation state. *Nat. Struct. Mol. Biol.* **20**, 1077–1084 (2013).
30. M. A. Carlson *et al.*, Ribosomal protein L7/L12 is required for GTPase translation factors EF-G, RF3, and IF2 to bind in their GTP state to 70S ribosomes. *FEBS J.* **284**, 1631–1643 (2017).
31. T. Uchiyumi, S. Honma, T. Nomura, E. R. Dabbs, A. Hachimori, Translation elongation by a hybrid ribosome in which proteins at the GTPase center of the *Escherichia coli* ribosome are replaced with rat counterparts. *J. Biol. Chem.* **277**, 3857–3862 (2002).
32. T. Nomura *et al.*, In vitro reconstitution of the GTPase-associated centre of the archaeobacterial ribosome: The functional features observed in a hybrid form with *Escherichia coli* 50S subunits. *Biochem. J.* **396**, 565–571 (2006).
33. H. Imai *et al.*, Functional role of the C-terminal tail of the archaeal ribosomal stalk in recruitment of two elongation factors to the sarcin/ricin loop of 23S rRNA. *Genes Cells* **20**, 613–624 (2015).
34. G. R. Heath, S. Scheuring, High-speed AFM height spectroscopy reveals  $\mu$ s-dynamics of unlabeled biomolecules. *Nat. Commun.* **9**, 4983 (2018).
35. T. Ando, T. Uchiyashi, N. Kodera, High-speed AFM and applications to biomolecular systems. *Annu. Rev. Biophys.* **42**, 393–414 (2013).
36. A. Rajendran, M. Endo, H. Sugiyama, Structural and functional analysis of proteins by high-speed atomic force microscopy. *Adv. Protein Chem. Struct. Biol.* **87**, 5–55 (2012).
37. T. Ando, T. Uchiyashi, S. Scheuring, Filming biomolecular processes by high-speed atomic force microscopy. *Chem. Rev.* **114**, 3120–3188 (2014).
38. Y. L. Lyubchenko, L. S. Shlyakhtenko, Imaging of DNA and protein-DNA complexes with atomic force microscopy. *Crit. Rev. Eukaryot. Gene Expr.* **26**, 63–96 (2016).
39. T. Ando, High-speed atomic force microscopy. *Curr. Opin. Chem. Biol.* **51**, 105–112 (2019).
40. G. R. Heath, S. Scheuring, Advances in high-speed atomic force microscopy (HS-AFM) reveal dynamics of transmembrane channels and transporters. *Curr. Opin. Struct. Biol.* **57**, 93–102 (2019).
41. K. Ito *et al.*, Molecular insights into the interaction of the ribosomal stalk protein with elongation factor  $1\alpha$ . *Nucleic Acids Res.* **42**, 14042–14052 (2014).
42. K. Maruyama *et al.*, Switch of the interactions between the ribosomal stalk and EF1A in the GTP- and GDP-bound conformations. *Sci. Rep.* **9**, 14761 (2019).
43. K. Baba, K. Tsurumura, I. Tanaka, M. Yao, T. Uchiyumi, Molecular dissection of the silkworm ribosomal stalk complex: The role of multiple copies of the stalk proteins. *Nucleic Acids Res.* **41**, 3635–3643 (2013).
44. L. Wawiórka *et al.*, Multiplication of ribosomal P-stalk proteins contributes to the fidelity of translation. *Mol. Cell. Biol.* **37**, e00060-17 (2017).
45. M. Mustafi, J. C. Weisshaar, Simultaneous binding of multiple EF-Tu copies to translating ribosomes in live *Escherichia coli*. *MBio* **9**, e02143-17 (2018).
46. C. Huang, C. S. Mandava, S. Sanyal, The ribosomal stalk plays a key role in IF2-mediated association of the ribosomal subunits. *J. Mol. Biol.* **399**, 145–153 (2010).
47. R. Murakami *et al.*, The interaction between the ribosomal stalk proteins and translation initiation factor 5B promotes translation initiation. *Mol. Cell. Biol.* **38**, e00067-18 (2018).
48. H. Imai *et al.*, The ribosomal stalk protein is crucial for the action of the conserved ATPase ABCE1. *Nucleic Acids Res.* **46**, 7820–7830 (2018).
49. T. Tanzawa *et al.*, The C-terminal helix of ribosomal P stalk recognizes a hydrophobic groove of elongation factor 2 in a novel fashion. *Nucleic Acids Res.* **46**, 3232–3244 (2018).
50. L. Wang *et al.*, A conserved proline switch on the ribosome facilitates the recruitment and binding of trGTPases. *Nat. Struct. Mol. Biol.* **19**, 403–410 (2012).
51. G. Raimo, M. Masullo, V. Bocchini, The interaction between the archaeal elongation factor 1alpha and its nucleotide exchange factor 1beta. *FEBS Lett.* **451**, 109–112 (1999).
52. T. Uchiyumi, K. Hori, T. Nomura, A. Hachimori, Replacement of L7/L12/L10 protein complex in *Escherichia coli* ribosomes with the eukaryotic counterpart changes the specificity of elongation factor binding. *J. Biol. Chem.* **274**, 27578–27582 (1999).
53. T. Ando *et al.*, A high-speed atomic force microscope for studying biological macromolecules. *Proc. Natl. Acad. Sci. U.S.A.* **98**, 12468–12472 (2001).
54. T. Uchiyashi, N. Kodera, T. Ando, Guide to video recording of structure dynamics and dynamic processes of proteins by high-speed atomic force microscopy. *Nat. Protoc.* **7**, 1193–1206 (2012).
55. K. X. Ngo, N. Kodera, E. Katayama, T. Ando, T. Q. P. Uyeda, Cofilin-induced unidirectional cooperative conformational changes in actin filaments revealed by high-speed atomic force microscopy. *eLife* **4**, 04806 (2015).
56. T. Uchiyashi, R. Iino, T. Ando, H. Noji, High-speed atomic force microscopy reveals rotary catalysis of rotorless F<sub>1</sub>-ATPase. *Science* **333**, 755–758 (2011).
57. T. Watanabe-Nakayama, K. Ono, High-speed atomic force microscopy of individual amyloidogenic protein assemblies. *Methods Mol. Biol.* **1814**, 201–212 (2018).